Letter

Operation Mechanism of Perovskite Quantum Dot Solar Cells Probed by Impedance Spectroscopy

Zahra Zolfaghari, Ehsan Hassanabadi, Didac Pitarch-Tena, Seog Joon Yoon, Zahra Shariatinia, Jao van de Lagemaat, Joseph M. Luther, and Ivan Mora-Seró

ACS Energy Lett., **Just Accepted Manuscript** • DOI: 10.1021/acsenergylett.8b02157 • Publication Date (Web): 10 Dec 2018

Operation Mechanism of Perovskite Quantum Dot Solar Cells Probed by Impedance Spectroscopy

*Zahra Zolfaghari,[1,2] Ehsan Hassanabadi,[1,3] Didac Pitarch-Tena,[1] Seog Joon Yoon,[1] Zahra Shariatinia,[2] Jao van de Lagemaat,[4] Joseph M. Luther[4] and Iván Mora-Seró,[1,]**

[1] Institute of Advanced Materials (INAM), Universitat Jaume I, Castellón de la Plana, Castellón, 12071, Spain

[2] Department of Chemistry, Amirkabir University of Technology (Tehran Polytechnic), Tehran, Iran

[3] Textile Engineering Department, Textile Excellence & Research Centers, Amirkabir University of Technology, Hafez Ave., Tehran 1591634311, Iran

[4] National Renewable Energy Laboratory, Golden, Colorado 80401, United States

*Corresponding author: sero@uji.es

ABSTRACT

We fabricated perovskite quantum dot solar cells (PQDSCs) varying the thickness of the QD layer by controlling the number of deposition cycles, that were systematically investigated with impedance spectroscopy. Despite the evident structural differences with respect to standard perovskite solar cells (PSCs), similar impedance spectra were obtained for PQDSCs, pointing to similar working principles in terms of the active layer. We distinguish two different regimes: at low illumination, recombination is ruled by multiple trapping with trap distributions and/or shunting. However, at higher light intensities Shockley-Read-Hall recombination is observed. In addition, the low frequency capacitance, C_{LF}, of PQDSCs increases several orders of magnitude by varying the illumination from dark to 1-sun conditions. This feature has not been observed in other kinds of photovoltaic devices and is characteristic of PSCs. Despite no consensus about the exact mechanism responsible for C_{LF} the suggested models point to an ion migration origin. Its observation in thin film and PQDSCs devices implies a similar effect in both.

TOC

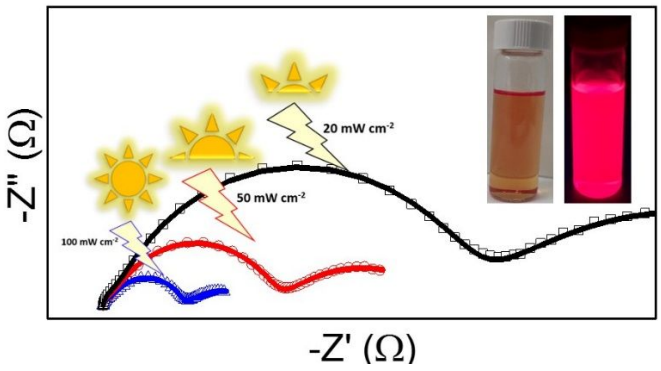

Halide perovskite solar cells (PSCs) have inspired the photovoltaic community in the last few years motivated by the high power conversion efficiency[1-3] already exceeding 23% for solution processed semiconductors.[4] This value surpasses other thin film photovoltaic technology efficiencies such as CdTe or CIGS and is close to that of crystalline Si cells.[4] However, the record efficiencies reported for hybrid organic-inorganic halide perovskites are in non-stabilized devices,[4] pointing to the most important challenge of halide perovskite technology: stability.[5] Although, hybrid perovskite solar cells show high efficiency, significant challenges remain to prove that a perovskite photovoltaic product can operate in the field with lifetime greater than 25 years as current technologies do.[6] One way to palliate these stability issues is the use of fully inorganic halide perovskites which provide higher stability under thermal stress.[7, 8] $CsPbI_3$ seems to be the most obvious all-inorganic choice to use in perovskite solar cells, as iodine perovskites presents a narrower bandgap than bromine and chlorine perovskites,[9, 10] consequently allowing light harvesting for a broader range of wavelengths. Nevertheless, the small size of Cs^+ cation makes the δ yellow orthorhombic phase with broad bandgap, E_g, the thermodynamically stable phase for $CsPbI_3$ at room temperature,[11] while the α perovskite phase with E_g =1.73 eV[12] is the stable phase at high temperature >320ºC.[13]

The limitation of the perovskite phase stability of $CsPbI_3$ bulk thin films can be overcome by the use of quantum dots (QDs) of the same material that can trap the crystal structure in the typically high temperature crystal perovskite phase.[13] Colloidal QDs are nanocrystals with smaller dimensions on the order of the Bohr exciton radius, allowing the observation of quantum confinement behaviors such as E_g tuning with particle size.[14] QDs have been broadly studied in the last few decades due to, among other things, their outstanding optical properties enhancing the reported ones for their bulk counterparts.[15, 16] The great success of halide perovskites boosted also the interest on the nanoparticles of these materials. Pérez-Prieto and coworkers reported by first time the development of hybrid halide perovskite nanoparticles,[17] and Kovalenko and coworkers prepared inorganic $CsPbX_3$ (X: Cl^-, Br^-, and/or I^-).[18] In addition to thin film halide perovskites, nanoparticles are also generating a huge interest as relative easy preparation methods yield a simple core structure, without need for passivating shells, reach photoluminescence quantum yield (PLQY) higher than 90%.[19, 20] This remarkable PLQY points to low non-radiative recombination and consequently shows excellent rationale for the development of solar cells. In fact, $CsPbI_3$ QDs have been deposited in a thin film utilized for solar cell fabrication recently

achieving a power conversion efficiency of 13.43%,[21] the world record efficiency for QD solar cells (QDSCs) already eclipsing any other QD material system with very little research.[4] This efficiency was achieved with a post treatment of perovskite QD film using halide salts which provide a method for tuning the coupling between perovskite QDs improving charge transport.[21] Lower performances have been obtained when iodine is totally or partially substituted by bromine.[22] $CsPbI_3$ QDs have been also used in QD sensitized solar cells configuration demonstrating a power conversion of efficiency of 5%.[23] In addition, perovskite QDs also offer the possibility of a real bandgap tuning using mixed halide perovskites, as $CsPb(Br_{1-x}I_x)_3$, as the reduced size of these nanoparticles avoids the phase segregation,[24] forming to bromide and iodine rich segregated domains.[25, 26] The phase segregation limits the effectiveness of high bandgap perovskite materials of special interest for the development of tandem devices.[27] It is also worth mentioning that QDs can exhibit E_g tuning by size confinement, enabling a potential higher bandgap material without the need for Br.

Despite this potential, to date there is little knowledge concerning the operating mechanism in perovskite QDs solar cells (PQDSCs) devices. A priori, the presence of complex QD surface structure[28] with the corresponding ligand molecules and presumed high densities of surface defects should influence transport and recombination, and therefore limit the open circuit potential, V_{oc}, to far below that of thin films. However, V_{oc} of up to 90% of the radiative limit have been shown in various compositions of PQD absorber layers,[5] and with hole transport contact optimization, voltage as large as 1.27 V have been reported for absorbers with E_g below 2 eV.[29] Here, we prepare PQDSCs with different QD layer thickness and characterize them systematically using frequency modulated Impedance spectroscopy (IS) to highlight the behavior of this system in terms of working mechanisms and in comparison with standard PSCs. IS can be applied at the device working conditions and the frequency modulation allows to decouple processes with different characteristic times making this technique ideal to characterize the different processes occurring in the device.[30]

$CsPbI_3$ QDs were synthesized following previous reports.[31] The synthesized QDs were cube shaped and 9.3 ± 1.5 nm in size as determined by TEM, see Figure S1. As reported previously, this synthesis procedure yields QDs in the perovskite crystalline phase as determined by XRD, see Figure S2. After QD deposition and subsequent ligand exchange, from the 0.39 theta at full width at half maximum (FWHM) of XRD peak corresponds to (100) plane, observed in the samples, Figure S2, a grain size of 21.46 nm is calculated using the Scherrer equation. As expected there is an increase of the crystal size after ligand exchange but with a size significantly lower that the reported in the standard solar

cells. On the other hand, we have previously reported that ligand exchange just partially remove the capping layer of QDs[32] preserving consequently the capping molecules and providing integrity to the perovskite nanoparticles. The PLQY of the $CsPbI_3$ QDs after a couple of washing processes, in order to remove the organic excess before the deposition, was measured to be roughly 40% in hexane solution. For the fabrication of PQDSCs, SnO_2:F (FTO) coated conductive glass was used as substrate. A compact layer of TiO_2 (c-TiO_2), was deposited as electron selective contact[33] on top of the FTO layer, see Figure 1a. A controlled number of layers of $CsPbI_3$ QDs were then spin coated on top of c-TiO_2 to vary the active layer thickness of the solar cell. More details about the fabrication process can be found in the Supporting Information. Briefly, a purified solution of $CsPbI_3$ QDs in octane was spin coated, then the film was dipped three times into a MeOAc or EtOAc solution containing $Pb(NO_3)_2$, rinsed in neat MeOAc or EtOAc, and then immediately dried with nitrogen. This complete process constitutes one layer of $CsPbI_3$ QDs and was repeated multiple times to create devices with different thickness ranging from 150 to 400 nm. On top of QD film, spiro-OMeTAD was deposited as hole selective contact. Finally, a 70 nm thick Au layer was evaporated as hole extracting contact. In Figure 1a the cross section of a PQDSC analyzed in this work is depicted.

The $CsPbI_3$ QD layer exhibits a photoluminescence (PL) at 689 nm with a full width at half maximum (FWHM) of 30 nm, see Figure 1b. As expected, the light absorption of the QD layers increases with the number of deposited layers, see Figure 1b. The thicknesses of the films were measured from the cross section by SEM, see Figure 1c. Different device batches have been produced and analyzed. Independent of the synthetic batch, the light absorption increased linearly with the number of deposited layers, in the case plotted in the inset of Figure 1c, the absorbance at 500 nm increased roughly by 0.3 for each 100 nm of QD layer thickness.

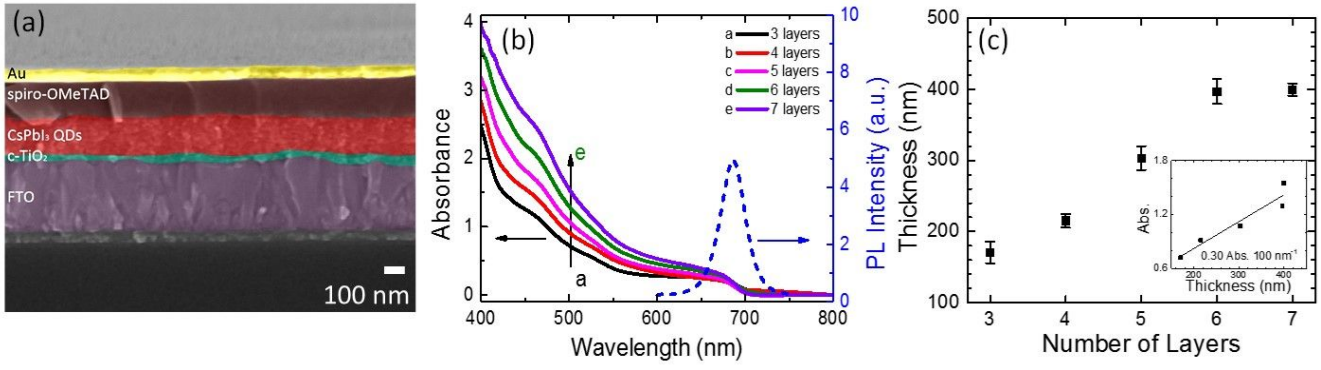

Figure 1. (a) SEM micrograph of the cross section of a PQDSC with an architecture glass/FTO/Compact TiO_2 (c-TiO_2)/$CsPbI_3$ QD thin film/spiro-OMeTAD/Au. (b) UV-Vis. absorption spectra (solid lines) of

PQDSCs with different number of deposited layers of $CsPbI_3$ and photoluminescence (dashed line). (c) Thickness of $CsPbI_3$ film as function of the number of deposited layers, measured by SEM. Inset, absorbance at 500 nm, see arrow in (b), as function of thickness, the slope of the linear fit is indicated.

Figure 2 shows the average photovoltaic parameters of the PQDSCs as function of the number of deposited layers, at least 5-10 cells have been prepared at each thickness. Photocurrent density, J_{sc}, and open circuit potential, V_{oc}, Figure 2a and 2b respectively, increased with the number of layer saturating for large numbers. J-V curves of representative devices with different number of layers are plotterd in Figure S3. On the other hand, fill factor, FF, remains practically constant with the number of layers taking into account the error bars. Consequently, the photoconversion efficiency, η, increased with the number of deposited QD layers until a maximum average efficiency is reached for 4 layers, in the conditions of preparation of the batch depicted in Figure 2. Further deposition of layers decreased the performance due mainly to the reduction of FF. In this study a maximum efficiency of 8.1 % was obtained with J_{SC}=11.3 mA/cm^2, V_{OC} = 1.094 V and FF= 66%, see Figure S4. Different batches have been prepared changing some deposition parameters such as the concentration of QDs, or the ligand exchange procedure. In all the analyzed batches the solar cell parameters exhibits the same trend as reported in Figure 2.

Comparing the performances obtained for PQDSCs with state-of-the-art PSCs based on bulk thin film,[3] FF and especially J_{SC} are significantly lower for PQDSCs. Higher FF have been reported for PQDSCs, ~80%,[21] in our case the low FF is probably due to the c-TiO_2 as this selective contact plays a fundamental role in the performance and FF of perovskite solar cells.[34] However, the weakest photovoltaic parameter for PQDSCs compared to conventional thin films is the photocurrent. J_{SC} has been improved by the use of cation halide salt treatment.[21] Nevertheless, this parameter still requiring improvement as the reported one for the record PQDSCs,[4] 15.246 mA/cm^2,[21] remains low in comparison with PSCs. This limitation is mainly due to the low incident photo to current efficiency (IPCE) at longer wavelengths, see Figure S5. Thin QD layers do not allow the complete harvesting of the long wavelength

region while an increase of thickness does not necessarily solve this issue as carrier transport limitations arise.

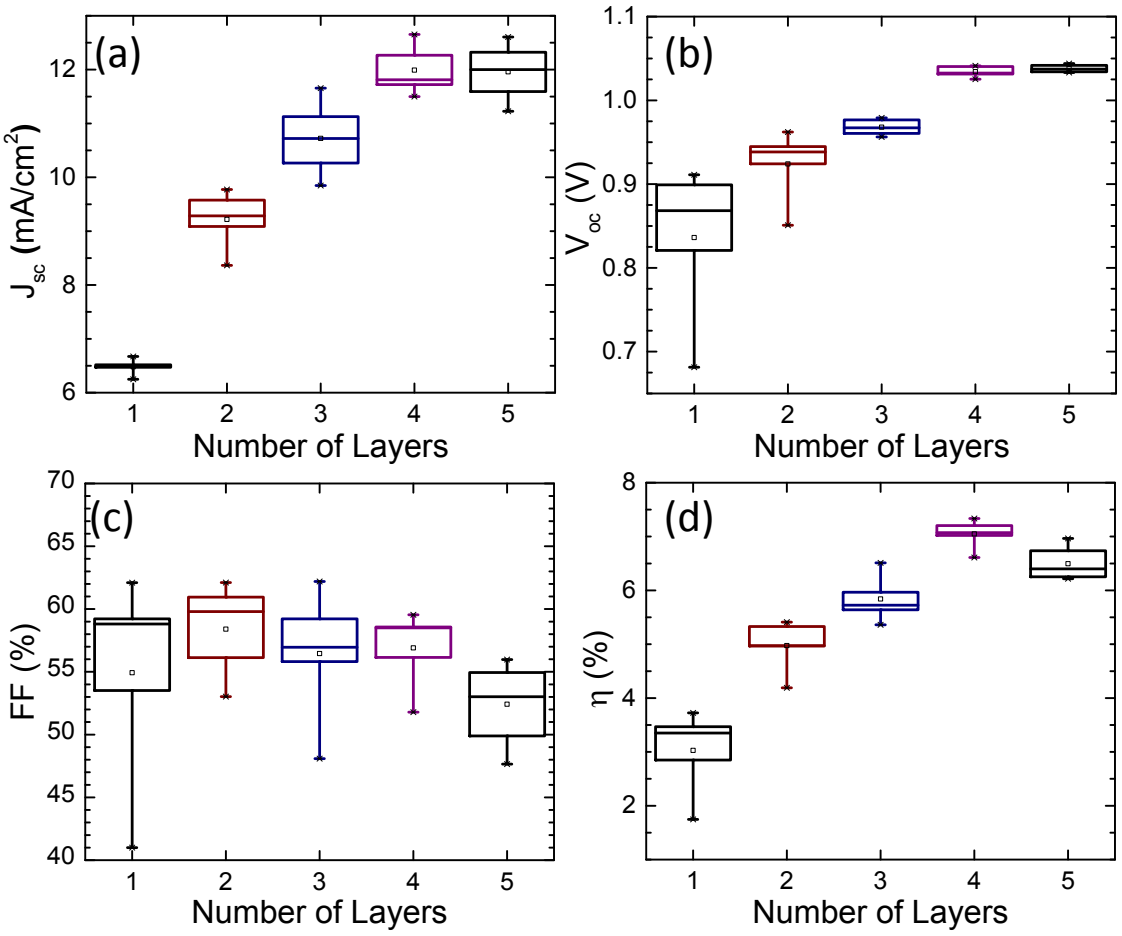

Figure 2. Average photovoltaic parameters of the PQDSCs prepared from a QD solution of 50 mg/ml as function of the number of deposited layers: (a) photocurrent, J_{SC}; (b) open circuit potential, V_{OC}; (c) fill factor, FF and (d) photoconversion efficiency, η.

In order to obtain a better understanding of PQDSCs, measurements at various light intensities were systematically performed. Details about the experimental procedure can be found in the supporting information and in the recent reference.[35] In Figure 3a, we plot V_{OC} as function of the light intensity. This representation allows for the easy calculation of the diode ideality factor, m, simply by the linear fit of

the data.[36] Figure 3a points to two different working regimes: at low and at high light intensities characterized by different ideality factors. At low light intensities *m* presents values significantly higher than two that could be assigned to a recombination process with multiple trapping events throughout a distribution of trap energies.[36] High *m* values have not been reported for standard PSCs using compact TiO_2 and spiro-OMeTAD respectively as electron and hole selective contacts[36, 37] and consequently this multiple trapping process at low light intensities would be associated with the perovskite QD layer. However, pinholes could also produce this high *m* behavior and this explanation cannot be completely ruled out especially in the case of the thinnest layers. At higher light intensities *m* reduced to two for the thickest samples as most of these traps are filled , pointing to an elimination of trapping leaving only Shockley-Read-Hall recombination at deep trap states.[36] Note that the small shunts produced by pinholes could be overwhelmed at hight illumination, and similar behavior should be expected. Pinholes are especially influencing in the cell performance for thinner samples in fact the thinnest layer in Figure 3a presents an ideally factor *m* is higher than 2 even at high illumination. Analysis of recombination resistance, see below, also points to the presence of pinholes especially in the case of the thinnest samples.

Impedance spectroscopy has been performed with an applied bias equal to V_{OC} under different light intensities.[35] While there is a lack of consensus on interpretation of such IS patterns, an interesting qualitative comparison can be performed to detect differences between PSCs and PQDSCs. As in the case of conventional thin film PSCs, two main features (arcs) at high and low frequency were presented in the Nyquist plot (imaginary part of the impedance, Z'', vs. real part of the impedance, Z'), [34, 38-40] see Figure 3b. A closer inspection of the Nyquist plot points to a more complex system, as the high frequency feature, the left handside feature with lower Z', is not a single arc but better represented as two merged arcs at high frequency.[34] Consequently, we have used an equivalent circuit previously employed for PSCs,[41] containing an intermediate frequency arc, to fit the experimental data, see Figure S6. This equivalent circuit model can accurately fit the experimental measurements, see Figure 3b. The impedance

spectra of PQDSCs are analogous to those observed for standard PSCs and consequently the same equivalent circuits can be used to simulate the performance of both devices.

Impedance fitting allows the comparison of different parameters as a function of the number of layers. Figure 3c plots the recombination resistance, R_{rec}, normalized to QD thin film volume for different PQDSCs obtained as the sum of low and high frequency resistances,[42, 43] more details in Figure S7. R_{rec} depends reversely to the recombination rate[30] and consequently can provide a direct quantitative view of the recombination process. R_{rec} can also be obtained as the lifetime divided by the chemical capacitance.[30] R_{rec} depends on carrier density and consequently on the applied bias , following a relation of the type[30]:

$$R_{rec} = R_0 \, exp\left(-\frac{\beta q V}{k_B T}\right) \qquad (1)$$

where R_0 is the recombination resistance at short circuit, q is the elementary charge, k_B is the Boltzmann constant, T is the absolute temperature and β a dimensionless parameter related with the ideality factor m as one is the inverted value of the other ($m=1/\beta$).[44] Good agreement is obtained between m and β values obtained in Figures 3a and 3c respectively, indicating the correctness of the experimental procedure.

From figure 3c, we find that the recombination resistance normalized to the volume of QD layer is improved as more layers are deposited up to saturation at 6 layers. This fact explains the increase in V_{oc} observed in Figure 2b by a reduction of the recombination rate as the deposition of multiple layers reduces potential pinholing and inhomogeneities.

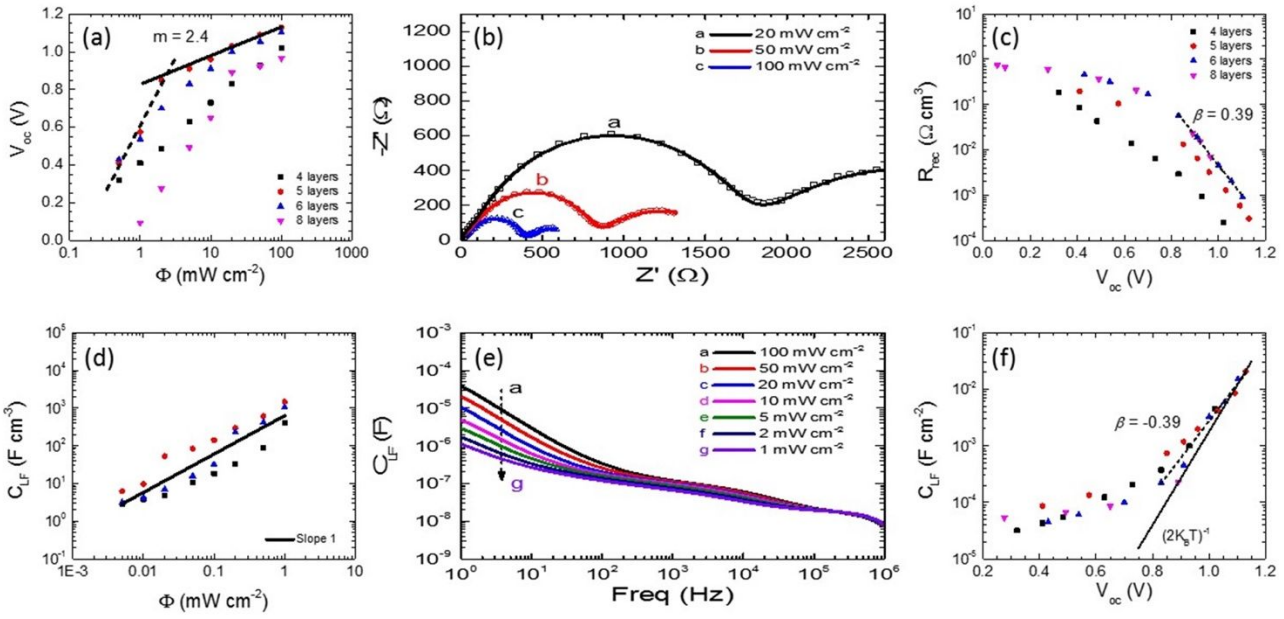

Figure 3. Optoelectronic characterization of PQDSCs with different thickness. (a) Open circuit potential as function of the light intensity. Solid line is a straight line with m = 2.4. (b) IS Nyquist plot at applied bias equal to the device V_{oc} for three different light intensities, symbols are experimental data while solid lines correspond to the fit using the equivalent circuit plotted in Figure S6. (c) Recombination resistance, R_{rec}, the dashed line is the linear regression of experimental points at high applied bias according Eq. (1) for the two thicker layers. Low frequency capacitance (d) as function of light intensity; (e) Bode plot at V_{oc} applied bias under different light intensities where dashed arrow indicate the evolution of the impedance spectra as light intensity is reduced and (f) C_{LF} as function of V_{OC}, the dashed line is the linear regression of experimental points at high applied bias while the solid line to representation of a straight line with slope defined by β=0.5.

Especially interesting is the characterization of low frequency capacitance, C_{LF}, as this capacitance is the most characteristic and recognizable feature of the impedance pattern of PSCs.[45] In PSCs, an increase in the C_{LF} of several orders of magnitude, even at zero applied bias, has been observed between dark conditions *vs.* 1-sun illuminations, in contrast with other photovoltaic technologies such as Si where a minimal change is observed.[45] On the other hand, C_{LF} is not observed in all-solid state dye sensitized solar cells either,[46] where the same selective contacts are used and consequently its origin is attributed to the perovskite layer and/or the interaction of the perovskite layer with the selective contacts. The physical origin of this capacitance is not clear and different models have been proposed. However,

many of these models, especially the most recent ones, coincide in pointing out the ionic migration as the fundamental origin of this phenomenon. On one hand, this capacitance has been associated with the accumulation of majority carriers at the TiO_2 interface, and it is observed at low frequency as the accumulation process is coupled with the ion migration.[47] On the other hand, light induced ion migration has been pointed out as the origin of the behavior.[48] In addition, the interplay between ionic and electronic charge transfer at perovskite-contact interfaces controlling electronic injection and recombination,[49] and ion-modulated recombination have been also indicated as possible origin of the behavior.[50] Consequently, there is a broad consensus on the ionic origin of this feature characterizing PSCs. Moreover, it has been reported that the J-V curve hysteresis observed for PSCs is related to ion migration,[50-53] and in fact a reduction of hysteresis has been related to a decrease of C_{LF}, connecting both effects with the ion migration behavior in halide perovskites.[50, 51, 54]

In the case of PQDSCs, it is notable to observe that the C_{LF} follows a similar behavior as in standard PSCs, exhibiting an linear increase of several orders of magnitude with light illumination, see Figure 3d. This behavior can be clearly observed at lower frequencies of the Bode plot of PQDSCs at applied bias equal to the V_{OC} at different light illuminations, see Figure 3e. This similatity strongly points to an analogous origin of C_{LF} in both PSCs and PQDSCs and origin linked with ion migration as it has been suggested for PSCs. However, further research is needed to fully confirm this point.

A close inspection of C_{LF} at different illuminations at V_{OC} conditions allows to differentiate two working regimes at low and high illumination, see Figure 3f. Note that in Figure 3f C_{LF} is normalized to the device area and not to the QD layer volume. At high light intensity all four devices present the same C_{LF} independent of the thickness, pointing to a process where interfacial effects take a major role. It is interesting to note that at high light intensities C_{LF} presents an exponential behavior, than can be fitted with a phenomenological equation analogous to Eq. (1):

$$C_{LF} = C_0 \, exp\left(-\frac{\beta q V}{k_B T}\right) \qquad (2)$$

where C_0 is the low frequency capacitance at 0 bias. A β = -0.39 is obtained for C_{LF} at high applied bias, see Figure 3f, while a complementary value of 0.39 was obtained for R_{rec} at high applied bias, see Figure 3c. Both β are in good agreement with the ideality factor measured independently in Figure 3a. On the other hand very similar values of β for the high and low resistances have been also obtained, see Figue S7. This complementarity of C_{LF} and R_{rec} slopes has been previously observed for standard PSCs,[42] where a of β = -0.5 was observed. A solid straight line corresponding to this β value is plotted in Figure 3e with a solid line for comparison. The β = -0.5 slope of the capacitance slope has been previously associated with the characteristic behavior of the interfacial charge accumulation.[42, 47, 55] The complementarity of the slopes points to a common effect linking recombination and ion migration through R_{rec} and C_{LF} respectively. It has been calculated that interstitial iodine defects introduce deep electron/hole traps in $CH_3NH_3PbI_3$,[56] if these defects are the main resposibles of non-radiative recombination process the recombination process would be affected by the ion migration, as the behavior R_{rec} and C_{LF} suggest. Note that two regimes can be also distinguished at for R_{rec} and C_{LF} at low and high applied bias, corresponding with the low and high regimes previously commented regarding the light intensity dependence in Figure 3a.

A further comparison between PQDSCs and PSCs can be performed taking into account the impedance measurements. A characteristic time, τ, can be defined as $C_{LF} \times R_{rec}$, see Figure S8. Note that τ is not a lifetime as C_{LF} is not a chemical capacitance.[57] Due to the complementary value of C_{LF} and R_{rec}, a value ~1 s is obtained, lower in the case of the thinner layer, see Figure S8. Characteristic times of the same order, measured by alternative transient techniques, have been reported for PSCs.[40, 58] This characteristic time has been shown independent of the applied bias and light illumination but decreasing

with the thickness and depending of the perovskite material and on the selective contacts.[42] The value of τ here obtained for PQDSC is very similar to that reported for planar PSCs of the same thickness fabricated and selective contacts with $MAPbI_3$ and one order of magnitude higher than planar cell of $FAPbI_3$, where MA is methylammonium and FA formamidinium. Additionally, PQDSCs present a τ 3 orders of magnitude higher than planar PSCs of the same thickness fabricated and selective contacts with $MAPbI_3$ but with inverted configuration and organic selective contacts.[42]

The impedance spectroscopy analysis of PQDSCs is remarkably similar to the most characteristics trends of standard PSCs, yet not observed in other cells: increase of several orders of magnitide of C_{LF} with light illumination, Figure 3d-e, complementary slopes of R_{rec} and C_{LF}, Figure 3c and 3f respectively, and nearly constant characteristic time $\tau = C_{LF} \cdot R_{rec}$, Figure S8. Consequently our study preliminarly suggest that the PQDSCs present the same working mechanism than PSCs.

It will be important to further confirm this preliminary results as important conclusions conclusions could be obtained from this similarity. Concretely, C_{LF} presents a similar behavior to the observed for PSCs, pointing to an important ion migration effect in PQDSCs, despite the fact that different ion migration properties might be expected between the PQDSCs and standard PSCs due to the structural differences between a thin film where QDs act as a brick with a continuous thin films with crystalline grains of hundreds of nanometers. It is expected that the presence of an organic capping on perovskite QD surface would likely influence the ion migration process in perovskite QD layers. In fact, there are anions on the QD surface just to balance the charge. Those anions could migrate under a field through the voids in the QD layer.[28] In our case, as ligands from the as-synthesized QDs were removed to reduce the interdot distance and to insolubilize the QDs on the substrate so that multiple layers could be coated.[31] Rapid and facile halide exchange in QD solutions has been observed due to the dynamic surface properties of QD perovskites in solution and this effect can be used to create homogeneous halide

alloy compositions.[59] Appropriate surface capping properties can reduce this effect.[60-62] The impedance analysis carried out in this work for PQDSCs shows clearly an analogous behavior than in standard PSCs for C_{LF}, usually attributed to ion migration as we have previously discussed. The implication in PQDSCs will need further research. In this sense, impedance spectroscopy arises as a highly appealing method for characterization of PQDSCs in general and ion migration in particular.

In summary, we have prepared and characterized PQDSCs with $CsPbI_3$ QDs. The devices with different number of QD deposited layers, *i.e.,* different thicknesses, have been prepared and analyzed. Two different working regimes are identified at low and high illumination conditions. At low illumination, recombination is ruled by multiple trapping and trap distributions. However, at higher light intensities most of these traps are filled observing a Shockley-Read-Hall recombination. PQDSCs present a similar impedance spectroscopy pattern than bulk thin film PSCs. Thick enough layers have to be prepared to reduce recombination which probably originated in thin layers due to non-uniformities. Interestingly, PQDSCs present the main impedance signature of PSCs, a high C_{LF} under illumination commonly related with ion migration. The similarity of the impedance pattern and the characteristic behavior of reported in this work of R_{rec} and C_{LF} strongly points to analogous working mechanism in both PSCs and PQDSCs. Further confirmation of this point would indicate that ionic effect is not just important in bulk perovskite thin films but on QD layer, influencing decisively the working behavior of PQDSCs. As in the case of PSCs at high illumination C_{LF} for PQDSCs is independent of the active layer thickness pointing to a major role of interfacial effects. C_{LF} also presents a complementary slope to the observed for R_{rec}, also observed in PSCs, pointing to a relationship between ion migration and recombination but further research is required to stablish properly this relationship. In addition, this work highlights the interest of impedance spectroscopy in the future optimization of this technology.

ASSOCIATED CONTENT

Supporting Information. Experimental methods including QD preparation and various characterizations are presented in the Supporting Information. TEM measurements. XRD analysis, champion cell J-V curve, IPCE, equivalent circuit.

AUTHOR INFORMATION

Corresponding Author

*Address correspondence to this author: sero@uji.es ; twitter: @IvanMoraSero

Notes

The authors declare no competing financial interest.

ACKNOWLEDGMENT

This work was partially supported by the European Research Council (ERC) via Consolidator Grant (724424 - No-LIMIT) and Generalitat Valenciana via Prometeo Grant Q-Devices (Prometeo/2018/098). We thank SCSI of University Jaume I for its help with TEM and XRD measurements. Additionally, this work was authored in part by the National Renewable Energy Laboratory, operated by Alliance for Sustainable Energy, LLC, for the U.S. Department of Energy (DOE) under Contract No. DE-AC36-08GO28308. Funding provided by U.S. Department of Energy Office of Energy Efficiency and Renewable Energy Solar Energy Technologies Office. The views expressed in the article do not necessarily represent the views of the DOE or the U.S. Government.

REFERENCES

1. Bella, F.; Griffini, G.; Correa-Baena, J. P.; Saracco, G.; Gratzel, M.; Hagfeldt, A.; Turri, S.; Gerbaldi, C. Improving Efficiency and Stability of Perovskite Solar Cells with Photocurable Fluoropolymers. *Science* **2016**, *354*, 203-206.
2. Yang, W. S.; Park, B.-W.; Jung, E. H.; Jeon, N. J.; Kim, Y. C.; Lee, D. U.; Shin, S. S.; Seo, J.; Kim, E. K.; Noh, J. H.; et al. Iodide Management in Formamidinium-Lead-Halide–Based Perovskite Layers for Efficient Solar cells. *Science* **2017**, *356*, 1376-1379.
3. Saliba, M.; Matsui, T.; Seo, J.-Y.; Domanski, K.; Correa-Baena, J.-P.; Nazeeruddin, M. K.; Zakeeruddin, S. M.; Tress, W.; Abate, A.; Hagfeldt, A.; et al. Cesium-Containing Triple Cation Perovskite Solar Cells: Improved Stability, Reproducibility and High Efficiency. *Energy Environ. Sci.* **2016**, *9*, 1989-1997.
4. https://www.nrel.gov/pv/assets/images/efficiency-chart-20180716.jpg
5. Christians, J. A.; Habisreutinger, S. N.; Berry, J. J.; Luther, J. M. Stability in Perovskite Photovoltaics: A Paradigm for Newfangled Technologies. *ACS Energy Lett.* **2018**, *3*, 2136-2143.
6. Conings B.; Drijkoningen J.; Gauquelin N.; Babayigit A.; D'Haen J.; D'Olieslaeger L.; Ethirajan A.; Verbeeck J.; Manca J.; Mosconi E.; et al. Intrinsic Thermal Instability of Methylammonium Lead Trihalide Perovskite. *Adv. Energy Mater.* **2015**, *5*, 1500477.
7. Sutton, R. J.; Eperon, G. E.; Miranda, L.; Parrott, E. S.; Kamino, B. A.; Patel, J. B.; Hörantner, M. T.; Johnston, M. B.; Haghighirad, A. A.; Moore, D. T.; et al. Bandgap-Tunable Cesium Lead Halide Perovskites with High Thermal Stability for Efficient Solar Cells. *Adv. Energy Mater.* **2016**, *6*, 1502458.
8. Kulbak, M.; Gupta, S.; Kedem, N.; Levine, I.; Bendikov, T.; Hodes, G.; Cahen, D. Cesium Enhances Long-Term Stability of Lead Bromide Perovskite-Based Solar Cells. *J. Phys. Chem. Lett.* **2016**, *7*, 167-172.
9. Suarez, B.; Gonzalez-Pedro, V.; Ripolles, T. S.; Sanchez, R. S.; Otero, L.; Mora-Sero, I. Recombination Study of Combined Halides (Cl, Br, I) Perovskite Solar Cells. *J. Phys. Chem. Lett.* **2014**, *5*, 1628-1635.
10. Noh, J. H.; Im, S. H.; Heo, J. H.; Mandal, T. N.; Seok, S. I. Chemical Management for Colorful, Efficient, and Stable Inorganic–Organic Hybrid Nanostructured Solar Cells. *Nano Lett.* **2013**, *13*, 1764-1769.
11. Eperon, G. E.; Paterno, G. M.; Sutton, R. J.; Zampetti, A.; Haghighirad, A. A.; Cacialli, F.; Snaith, H. J. Inorganic Caesium Lead Iodide Perovskite Solar Cells. *J. Mater. Chem. A* **2015**, *3*, 19688-19695.
12. Eperon, G. E.; Stranks, S. D.; Menelaou, C.; Johnston, M. B.; Herz, L. M.; Snaith, H. J. Formamidinium Lead Trihalide: A Broadly Tunable Perovskite for Efficient Planar Heterojunction Solar Cells. *Energy Environ. Sci.* **2014**, *7*, 982-988.
13. Sharma, S.; Weiden, N.; Weiss, A. Phase Diagrams of Quasibinary Systems of the Type: ABX_3–$A'BX_3$; ABX_3–$AB'X_3$, and ABX_3–ABX'_3; X = Halogen. *Z. Phys. Chem.* **1992**, *175*, 63-80.
14. Alivisatos, A. P. Semiconductor Clusters, Nanocrystals, and Quantum Dots. *Science* **1996**, *271*, 933-937.
15. Kovalenko, M. V.; Manna, L.; Cabot, A.; Hens, Z.; Talapin, D. V.; Kagan, C. R.; Klimov, V. I.; Rogach, A. L.; Reiss, P.; Milliron, D. J.; et al. Prospects of Nanoscience with Nanocrystals. *ACS nano* **2015**, *9*, 1012-1057.
16. Owen, J.; Brus, L. Chemical Synthesis and Luminescence Applications of Colloidal Semiconductor Quantum Dots. *J. Am. Chem. Soc.* **2017**, *139*, 10939-10943.
17. Schmidt, L. C.; Pertegás, A.; González-Carrero, S.; Malinkiewicz, O.; Agouram, S.; Mínguez Espallargas, G.; Bolink, H. J.; Galian, R. E.; Pérez-Prieto, J. Nontemplate Synthesis of $CH_3NH_3PbBr_3$ Perovskite Nanoparticles. *J. Am. Chem. Soc.* **2014**, *136*, 850-853.
18. Protesescu, L.; Yakunin, S.; Bodnarchuk, M. I.; Krieg, F.; Caputo, R.; Hendon, C. H.; Yang, R. X.; Walsh, A.; Kovalenko, M. V. Nanocrystals of Cesium Lead Halide Perovskites ($CsPbX_3$, X = Cl, Br, and I): Novel Optoelectronic Materials Showing Bright Emission with Wide Color Gamut. *Nano Lett.* **2015**, *15*, 3692-3696.
19. Kovalenko, M. V.; Protesescu, L.; Bodnarchuk, M. I. Properties and Potential Optoelectronic Applications

of Lead Halide Perovskite Nanocrystals. *Science* **2017**, *358*, 745-750.
20. Huang, H.; Bodnarchuk, M. I.; Kershaw, S. V.; Kovalenko, M. V.; Rogach, A. L. Lead Halide Perovskite Nanocrystals in the Research Spotlight: Stability and Defect Tolerance. *ACS Energy Lett.* **2017**, *2*, 2071-2083.
21. Sanehira, E. M.; Marshall, A. R.; Christians, J. A.; Harvey, S. P.; Ciesielski, P. N.; Wheeler, L. M.; Schulz, P.; Lin, L. Y.; Beard, M. C.; Luther, J. M. Enhanced Mobility $CsPbI_3$ Quantum Dot Arrays for Record-Efficiency, High-Voltage Photovoltaic Cells. *Sci. Adv.* **2017**, *3*, eaao4204.
22. Ghosh, D.; Ali, M. Y.; Chaudhary, D. K.; Bhattacharyya, S. Dependence of Halide Composition on the Stability of Highly Efficient All-Inorganic Cesium Lead Halide Perovskite Quantum Dot Solar Cells. *Sol. Energy Mater. Sol. Cells* **2018**, *185*, 28-35.
23. Liu, F.; Zhang, Y.; Ding, C.; Toyoda, T.; Ogomi, Y.; Ripolles, T. S.; Hayase, S.; Minemoto, T.; Yoshino, K.; Dai, S.; et al. Ultrafast Electron Injection from Photoexcited Perovskite $CsPbI_3$ QDs into TiO_2 Nanoparticles with Injection Efficiency near 99%. *J. Phys. Chem. Lett.* **2018**, *9*, 294-297.
24. Draguta, S.; Sharia, O.; Yoon, S. J.; Brennan, M. C.; Morozov, Y. V.; Manser, J. S.; Kamat, P. V.; Schneider, W. F.; Kuno, M. Rationalizing the Light-Induced Phase Separation of Mixed Halide Organic-Inorganic Perovskites. *Nat. Commun.* **2017**, *8*, 200.
25. Hoke, E. T.; Slotcavage, D. J.; Dohner, E. R.; Bowring, A. R.; Karunadasa, H. I.; McGehee, M. D. Reversible Photo-Induced Trap Formation in Mixed-Halide Hybrid Perovskites for Photovoltaics. *Chem. Sci.* **2015**, *6*, 613-617.
26. Gualdrón-Reyes, A. F.; Yoon, S. J.; Mora-Seró, I. Recent Insights for Achieving Mixed Halide Perovskites without Halide Segregation. *Curr. Opin. Electrochem.* **2018**, DOI: 10.1016/j.coelec.2018.09.007.
27. Yang, T. C.-J.; Fiala, P.; Jeangros, Q.; Ballif, C. High-Bandgap Perovskite Materials for Multijunction Solar Cells. *Joule* **2018**, *2*, 1421-1436.
28. Wheeler, L. M.; Sanehira, E. M.; Marshall, A. R.; Schulz, P.; Suri, M.; Anderson, N. C.; Christians, J. A.; Nordlund, D.; Sokaras, D.; Kroll, T.; et al. Targeted Ligand-Exchange Chemistry on Cesium Lead Halide Perovskite Quantum Dots for High-Efficiency Photovoltaics. *J. Am. Chem. Soc.* **2018**, *140*, 10504-10513.
29. Yuan, J.; Ling, X.; Yang, D.; Li, F.; Zhou, S.; Shi, J.; Qian, Y.; Hu, J.; Sun, Y.; Yang, Y.; et al. Band-Aligned Polymeric Hole Transport Materials for Extremely Low Energy Loss α-$CsPbI_3$ Perovskite Nanocrystal Solar Cells. *Joule* **2018**, *2*, 2450-2463.
30. Fabregat-Santiago, F.; Garcia-Belmonte, G.; Mora-Seró, I.; Bisquert, J. Characterization of Nanostructured Hybrid and Organic Solar Cells by Impedance Spectroscopy. *Phys. Chem. Chem. Phys.* **2011**, *13*, 9083–9118.
31. Swarnkar, A.; Marshall, A. R.; Sanehira, E. M.; Chernomordik, B. D.; Moore, D. T.; Christians, J. A.; Chakrabarti, T.; Luther, J. M. Quantum Dot–Induced Phase Stabilization of α-$CsPbI_3$ Perovskite for High-Efficiency Photovoltaics. *Science* **2016**, *354*, 92-95.
32. Gualdrón-Reyes, A. F.; Yoon, S. J.; Barea, E. M.; Agouram, S.; Muñoz-Sanjosé, V.; Meléndez, Á. M.; Niño-Gómez, M. E.; Mora-Seró, I. Controlling the Phase Segregation in Mixed Halide Perovskites through Nanocrystal Size. *ACS Energy Lett.* **2019**, *4*, 54-62.
33. Fakharuddin, A.; Schmidt-Mende, L.; Garcia-Belmonte, G.; Jose, R.; Mora-Sero, I. Interfaces in Perovskite Solar Cells. *Adv. Energy Mater.* **2017**, *7*, 1700623.
34. Juarez-Perez, E. J.; Wuβler, M.; Fabregat-Santiago, F.; Lakus-Wollny, K.; Mankel, E.; Mayer, T.; Jaegermann, W.; Mora-Sero, I. Role of the Selective Contacts in the Performance of Lead Halide Perovskite Solar Cells. *J. Phys. Chem. Lett.* **2014**, *5*, 680-685.
35. Pitarch-Tena, D.; Ngo, T. T.; Vallés-Pelarda, M.; Pauporté, T.; Mora-Seró, I. Impedance Spectroscopy Measurements in Perovskite Solar Cells: Device Stability and Noise Reduction. *ACS Energy Lett.* **2018**, *3*, 1044-1048.
36. Tress, W.; Yavari, M.; Domanski, K.; Yadav, P.; Niesen, B.; Correa Baena, J. P.; Hagfeldt, A.; Graetzel, M. Interpretation and Evolution of Open-Circuit Voltage, Recombination, Ideality Factor and Subgap

Defect States during Reversible Light-Soaking and Irreversible Degradation of Perovskite Solar Cells. *Energy Environ. Sci.* **2018**, *11*, 151-165.
37. Contreras-Bernal, L.; Salado, M.; Todinova, A.; Calio, L.; Ahmad, S.; Idígoras, J.; Anta, J. A. Origin and Whereabouts of Recombination in Perovskite Solar Cells. *J. Phys. Chem. C* **2017**, *121*, 9705-9713.
38. Dualeh, A.; Moehl, T.; Tétreault, N.; Teuscher, J.; Gao, P.; Nazeeruddin, M. K.; Grätzel, M. Impedance Spectroscopic Analysis of Lead Iodide Perovskite-Sensitized Solid-State Solar Cells. *ACS nano* **2014**, *8*, 362-373.
39. Pascoe, A. R.; Duffy, N. W.; Scully, A. D.; Huang, F.; Cheng, Y. B. Insights into Planar $CH_3NH_3PbI_3$ Perovskite Solar Cells Using Impedance Spectroscopy. *J. Phys. Chem. C* **2015**, *119*, 4444-4453.
40. Pockett, A.; Eperon, G. E.; Peltola, T.; Snaith, H. J.; Walker, A.; Peter, L. M.; Cameron, P. J. Characterization of Planar Lead Halide Perovskite Solar Cells by Impedance Spectroscopy, Open-Circuit Photovoltage Decay, and Intensity-Modulated Photovoltage/Photocurrent Spectroscopy. *J. Phys. Chem. C* **2015**, *119*, 3456-3465.
41. Guerrero, A.; Garcia-Belmonte, G.; Mora-Sero, I.; Bisquert, J.; Kang, Y. S.; Jacobsson, T. J.; Correa-Baena, J.-P.; Hagfeldt, A. Properties of Contact and Bulk Impedances in Hybrid Lead Halide Perovskite Solar Cells Including Inductive Loop Elements. *J. Phys. Chem. C* **2016**, *120*, 8023-8032.
42. Zarazua, I.; Han, G.; Boix, P. P.; Mhaisalkar, S.; Fabregat-Santiago, F.; Mora-Seró, I.; Bisquert, J.; Garcia-Belmonte, G. Surface Recombination and Collection Efficiency in Perovskite Solar Cells from Impedance Analysis. *J. Phys. Chem. Lett.* **2016**, *7*, 5105-5113.
43. Zarazúa, I.; Sidhik, S.; Lopéz-Luke, T.; Esparza, D.; De la Rosa, E.; Reyes-Gomez, J.; Mora-Seró, I.; Garcia-Belmonte, G. Operating Mechanisms of Mesoscopic Perovskite Solar Cells through Impedance Spectroscopy and J–V Modeling. *J. Phys. Chem. Lett.* **2017**, *8*, 6073-6079.
44. Ansari-Rad, M.; Abdi, Y.; Arzi, E. Reaction Order and Ideality Factor in Dye-Sensitized Nanocrystalline Solar Cells: A Theoretical Investigation. *J. Phys. Chem. C* **2012**, *116*, 10867-10872.
45. Juarez-Perez, E. J.; Sanchez, R. S.; Badia, L.; Garcia-Belmonte, G.; Kang, Y. S.; Mora-Sero, I.; Bisquert, J. Photoinduced Giant Dielectric Constant in Lead Halide Perovskite Solar Cells. *J. Phys. Chem. Lett.* **2014**, *5*, 2390-2394.
46. Fabregat-Santiago, F.; Bisquert, J.; Cevey, L.; Chen, P.; Wang, M.; Zakeeruddin, S. M.; Grätzel, M. Electron Transport and Recombination in Solid-State Dye Solar Cell with Spiro-OMeTAD as Hole Conductor. *J. Am. Chem. Soc.* **2009**, *131*, 558-562.
47. Zarazua, I.; Bisquert, J.; Garcia-Belmonte, G. Light-Induced Space-Charge Accumulation Zone as Photovoltaic Mechanism in Perovskite Solar Cells. *J. Phys. Chem. Lett.* **2016**, *7*, 525-528.
48. Bag, M.; Renna, L. A.; Adhikari, R. Y.; Karak, S.; Liu, F.; Lahti, P. M.; Russell, T. P.; Tuominen, M. T.; Venkataraman, D. Kinetics of Ion Transport in Perovskite Active Layers and Its Implications for Active Layer Stability. *J. Am. Chem. Soc.* **2015**, *137*, 13130-13137.
49. Moia, D.; Gelmetti, I.; Calado, P.; Fisher, W.; Stringer, M.; Game, O.; Hu, Y.; Docampo, P.; Lidzey, D.; Palomares, E.; et al. Ionic-to-Electronic Current Amplification in Hybrid Perovskite Solar Cells. *arXiv.org, e-Print Arch., Phys*. **2018**, 1805.06446v2.
50. Jacobs, D. A.; Shen, H.; Pfeffer, F.; Peng, J.; White, T. P.; Beck, F. J.; Catchpole, K. R. The Two Faces of Capacitance: New Interpretations for Electrical Impedance Measurements of Perovskite Solar Cells and Their Relation to Hysteresis. *arXiv.org, e-Print Arch., Phys.* **2018**, 1807.00954v1.
51. Kim, H.-S.; Jang, I.-H.; Ahn, N.; Choi, M.; Guerrero, A.; Bisquert, J.; Park, N.-G. Control of I–V Hysteresis in $CH_3NH_3PbI_3$ Perovskite Solar Cell. *J. Phys. Chem. Lett.* **2015**, *6*, 4633-4639.
52. Snaith, H. J.; Abate, A.; Ball, J. M.; Eperon, G. E.; Leijtens, T.; Noel, N. K.; Stranks, S. D.; Wang, J. T.-W.; Wojciechowski, K.; Zhang, W. Anomalous Hysteresis in Perovskite Solar Cells. *J. Phys. Chem. Lett.* **2014**, *5*, 1511-1515.
53. Tress, W.; Marinova, N.; Moehl, T.; Zakeeruddin, S. M.; Nazeeruddin, M. K.; Gratzel, M. Understanding the Rate-Dependent J–V Hysteresis, Slow Time Component, and Aging in $CH_3NH_3PbI_3$ Perovskite Solar Cells: The Role of a Compensated Electric Field. *Energy Environ. Sci.* **2015**, *8*, 995-1004.

54. Anaya, M.; Zhang, W.; Hames, B. C.; Li, Y.; Fabregat-Santiago, F.; Calvo, M. E.; Snaith, H. J.; Miguez, H.; Mora-Sero, I. Electron Injection and Scaffold Effects in Perovskite Solar Cells. *J. Mater. Chem. C* **2017**, *5*, 634-644.
55. Contreras, L.; Idigoras, J.; Todinova, A.; Salado, M.; Kazim, S.; Ahmad, S.; Anta, J. A. Specific Cation Interactions as the Cause of Slow Dynamics and Hysteresis in Dye and Perovskite Solar Cells: A Small-Perturbation Study. *Phys. Chem. Chem. Phys.* **2016**, *18*, 31033-31042.
56. Meggiolaro, D.; Motti, S. G.; Mosconi, E.; Barker, A. J.; Ball, J.; Andrea Riccardo Perini, C.; Deschler, F.; Petrozza, A.; De Angelis, F., Iodine Chemistry Determines the Defect Tolerance of Lead-Halide Perovskites. *Energy Environ. Sci.* **2018**, *11*, 702-713.
57. Bisquert, J.; Fabregat-Santiago, F.; Mora-Seró, I.; Garcia-Belmonte, G.; Giménez, S. Electron Lifetime in Dye-Sensitized Solar Cells: Theory and Interpretation of Measurements. *J. Phys. Chem. C* **2009**, *113*, 17278–17290.
58. Sanchez, R. S.; Gonzalez-Pedro, V.; Lee, J.-W.; Park, N.-G.; Kang, Y. S.; Mora-Sero, I.; Bisquert, J. Slow Dynamic Processes in Lead Halide Perovskite Solar Cells. Characteristic Times and Hysteresis. *J. Phys. Chem. Lett.* **2014**, *5*, 2357-2363.
59. Nedelcu, G.; Protesescu, L.; Yakunin, S.; Bodnarchuk, M. I.; Grotevent, M. J.; Kovalenko, M. V. Fast Anion-Exchange in Highly Luminescent Nanocrystals of Cesium Lead Halide Perovskites ($CsPbX_3$, X = Cl, Br, I). *Nano Lett.* **2015**, *15*, 5635-5640.
60. Krieg, F.; Ochsenbein, S. T.; Yakunin, S.; ten Brinck, S.; Aellen, P.; Süess, A.; Clerc, B.; Guggisberg, D.; Nazarenko, O.; Shynkarenko, Y.; et al. Colloidal $CsPbX_3$ (X = Cl, Br, I) Nanocrystals 2.0: Zwitterionic Capping Ligands for Improved Durability and Stability. *ACS Energy Lett.* **2018**, *3*, 641-646.
61. Ravi, V. K.; Scheidt, R. A.; DuBose, J.; Kamat, P. V. Hierarchical Arrays of Cesium Lead Halide Perovskite Nanocrystals through Electrophoretic Deposition. *J. Am. Chem. Soc.* **2018**, 140, 8887-8894.
62. Ravi, V. K.; Scheidt, R. A.; Nag, A.; Kuno, M.; Kamat, P. V. To Exchange or Not to Exchange. Suppressing Anion Exchange in Cesium Lead Halide Perovskites with $PbSO_4$–Oleate Capping. *ACS Energy Lett.* **2018**, *3*, 1049-1055.

SUPPORTING INFORMATION

Operation Mechanism of Perovskite Quantum Dot Solar Cells Probed by Impedance Spectroscopy

*Zahra Zolfaghari,[1,2] Ehsan Hassanabadi,[1,3] Didac Pitarch-Tena,[1] Seog Joon Yoon,[1] Zahra Shariatinia,[2] Jao van de Lagemaat,[4] Joseph M. Luther[4] and Iván Mora-Seró,[1,]**

[1] Institute of Advanced Materials (INAM), Universitat Jaume I, Castellón de la Plana, Castellón, 12071, Spain

[2] Department of Chemistry, Amirkabir University of Technology (Tehran Polytechnic), Tehran, Iran

[3] Textile Engineering Department, Textile Excellence & Research Centers, Amirkabir University of Technology, Hafez Ave., Tehran 1591634311, Iran

[4] National Renewable Energy Laboratory, Golden, Colorado 80401, United States

*Corresponding author: sero@uji.es

Experimental Section

Materials

Cesium carbonate (Cs_2CO_3; 99.9 %, Sigma-Aldrich), PbI_2 (99.999 %, ABCR), oleic acid (OA; 90 %, Sigma-Aldrich), oleylamine (OAM; ≥ 98 %, Sigma-Aldrich), 1-octadecene (ODE; 90 %, Sigma-Aldrich), hexane (≥ 95 %, Sigma-Aldrich), octane (≥ 99 %, Sigma-Aldrich), Methyl acetate(MeOAc anhydrous, 99.5 %, Sigma-Aldrich), Eethyl acetate (EtOAc anhydrous, 99.8 %,Sigma-Aldrich), $Pb(NO_3)_2$ (99.999 %, Sigma-Aldrich), $N^2,N^2,N^{2'},N^{2'},N^7,N^7,N^{7'},N^{7'}$-octakis(4-methoxyphenyl)-9,9′-spirobi[9H-fluorene]-2,2′,7,7′-tetramine (spiro-OMeTAD, ≥ 99 %, Merck), cholorobenzene (anhydrous, 99.8 %, Sigma-Aldrich), 4-tert-butylpridine (4-TBP; 96 %, Sigma-Aldrich), bis (trifluoromethane)-sulfonimide lithium salt (99.95 %, Sigma-Aldrich), acetonitrile (anhydrous, 99.8 %, Sigma-Aldrich), and commercial Ti-alkoxide solution (ShareChem, SC-BT060). FTO glasses (25x25 mm, Pilkington TEC15, ~15$\Omega\square^{-1}$). All materials were used as recived.

$CsPbI_3$ QDs synthesis and purification

$CsPbI_3$ QDs were synthesized following the report by Luther and coworkers[1]. Cs-oleate in ODE solution was synthesized with 0.814 g of Cs_2CO_3, 2.5 ml of oleic acid, and 40 ml of ODE in 100-ml three-neck flask under vacuum at 120 ˚C for 1 hr under stirring. After purging the nitrogen in the flask, the flask was heated to 150 ˚C until the reaction was completed shown clear solution. The Cs-oleate in ODE solution was cooled and used for QD synthesis. In order to synthesize $CsPbI_3$ QDs, 0.5 g of PbI_2 and 25 ml of ODE were degassed in the 100 ml three neck flask under vacuum at 120 ˚C for 30 min under stirring. OA and OAM (2.5 ml of each) were added to the reaction flask and put flask under vacuum for 1 minute until the PbI_2 had completely dissolved. Then, PbI_2 solution was purged with N_2 and then heated to 170 ˚C quickly. Once the reaction temperature was reached, 2 ml of preheated Cs-Oleate in ODE (100˚C) was injected into the reaction flask. The reaction was quenched by immediate immersion of the flask into an ice-water bath (5 sec after injection). To purify QDs, 70 ml of MeOAc or EtOAc was added to as-synthesized QD solution and then centrifuged at 4700 rpm for 5 min. The supernatant was discarded, and the QDs was dispersed again in 5 ml of hexane. 8 ml of MeOAc or EtOAc was added again to QDs solution and then immediately centrifuged at 4700 rpm for 5 min. the precipitate was dispersed in 10 ml of hexane. QDs solution was kept to dark at 4 ˚C.

Before use, the solution was centrifuged 4700 rpm for 5 min, the precipitate was removed and the QDs was dried with nitrogen and dissolved in octane at concentration of ~50 and 75 mg/ml.

Device fabrication

A ~30 nm compact TiO_2 layer was deposited via solution onto FTO. 80 µL of Ti-alkoxide solution was deposited with spin coating at 4000 rpm for 30 seconds, the spin-cast films were dried at 150 ˚C for 10 min and then annealed at 500 ˚C for 30 min. $CsPbI_3$ QDs film were fabricated according to previous report.[1] In short, saturated $Pb(NO_3)_2$ in MeOAc or EtOAc was prepared by sonicating 40 mg of $Pb(NO_3)_2$ in 40 ml of MeOAc or EtOAc for 10 min and then for removing the excess salt it was centrifuged at 4000 rpm for 5 min. Each layer of $CsPbI_3$ QDs was spin coated from QDs solution in octane (50 mg/ml and 75 mg/ml) at spin speed of 1000 rpm for 20 s and 2000 rpm for 5 s. Then, the film was dipped 3 times into $Pb(NO_3)_2$ in MeOAc or EtOAc solution, rinsed in neat MeOAc or EtOAc , and then immediately dried with nitrogen. Devices were prepared with different layer 1-5 of 50 mg/ml and 1-7 of 75 mg/ml solution. The spiro-OMeTAD hole transporting material was spin coating at 4000 rmp for 30 sec from a solution of 72.3 mg of spiro-OMeTAD, 1 ml chlorobenzene, 28.8 µL of 4-TBP, and 17.5 µL of Li-TFSI solution (520 mg/ml in acetonitrile). Au was evaporated at rate ranging from 0.5-1 A/s for a total thickness of 70 nm.

Characterizations

The current- voltage were measured through Abet Technologies Sun 2000 Class A solar simulator with a Keithley 2612 Source Meter with scan rate of 10 mV/s under AM 1G. The active area of the device was defined based on a mask area of 0.11 cm^{-2}. The light intensity was matched one sun by calibrating with a Si reference cell equipped with a IR-cut off filter. IPCE measurement was measured with employing 150 W xenon lamp coupled with a monochromator. The external quantum efficiency was measured using an optical power meter 70310 from Oriel instruments, using Si photodiode to calibrate the system. FE-SEM (JSM7001F) was utilized to carry out thickness of film. The structural of the $CsPbI_3$ QDs was determined by using X-ray diffractometer (Bruker AXS, D4 Endeavor advanced X-ray diffractometer, with Cu Kα radiation). Absorbance was done using Varian Cary 300 Bio spectrophotometer. PLQY was measured using a Hamamatsu integrating sphere where a quartz cuvette containing the sample

was placed. PLQY is referred to QDs which were purified two times with methyl acetate were dispersed in hexane. For PLQY measurement, we the absorbance of QDs solution was kept between 0.5-0.6. As reference, measurement was performed with cuvette containing only the hexane in the same excitation wavelength. PLQY of $CsPbI_3$ QDs solution with absorbance of 0.553 at excitation wavelength of 400 nm is 40%. PL was measured by Horiba FL-100. PLQY was measured with an integrating sphere with excitation wavelength at 400 nm. The impedance spectroscopy measurements were carried out in a PGSTAT- 30 potentiostat from Autolab. A Xe lamp was used to illuminate the PSC controlling the light intensity with neutral density filters, between 0.1 and 100 mW/cm^2 in a logarithmic scale. The AC voltage perturbation was fixed at 20 mV under open-circuit conditions. The integration time was fixed at 0.125 s and the number of cycles was equal to 1. Each frequency spectrum was measured ranging between 1 MHz and 0.1 Hz. The equivalent circuit we have used to fit the data is plotted in Figure S5. Further details on Impedance characterization method can be found in reference [2].

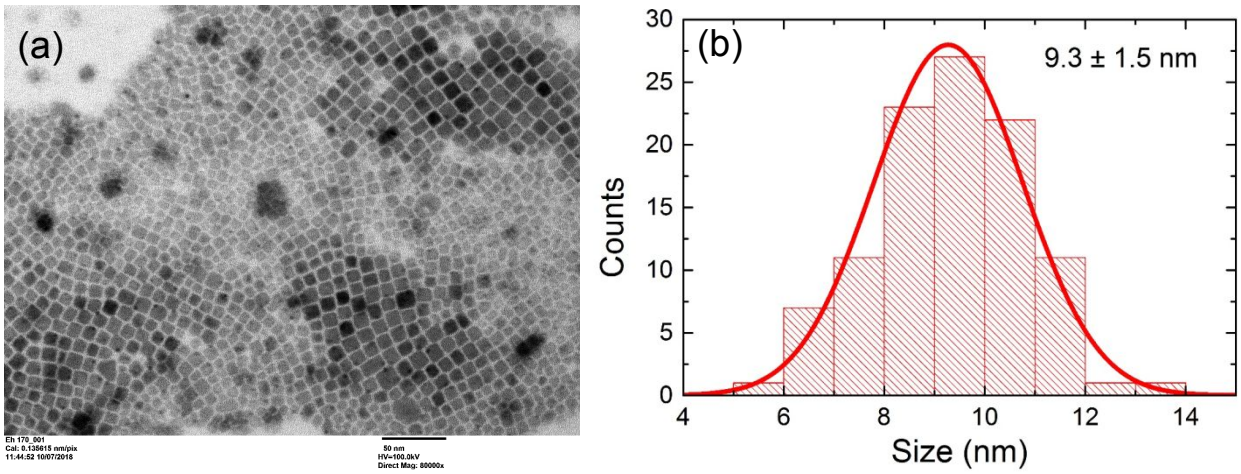

Figure S1. (a) TEM image of $CsPbI_3$ QDs and (b) their diameter distributions (9.3 ± 1.5 nm).

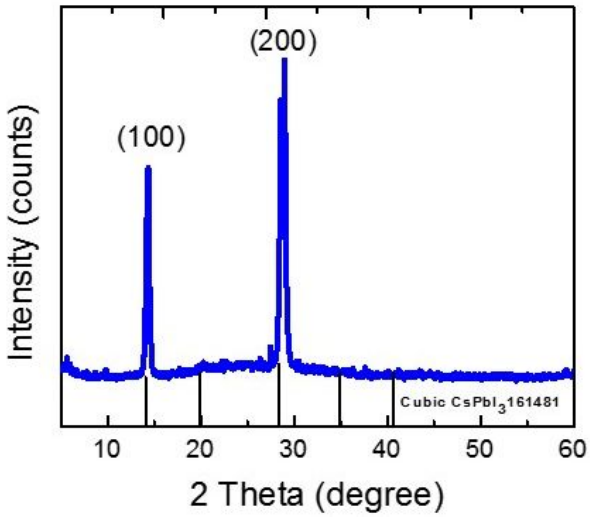

Figure S2. XRD pattern of $CsPbI_3$ QDs (blue solid line). For comparison diffractions from cubic $CsPbI_3$, crystallographic data ICSD-161481, are also included (black solid lines).

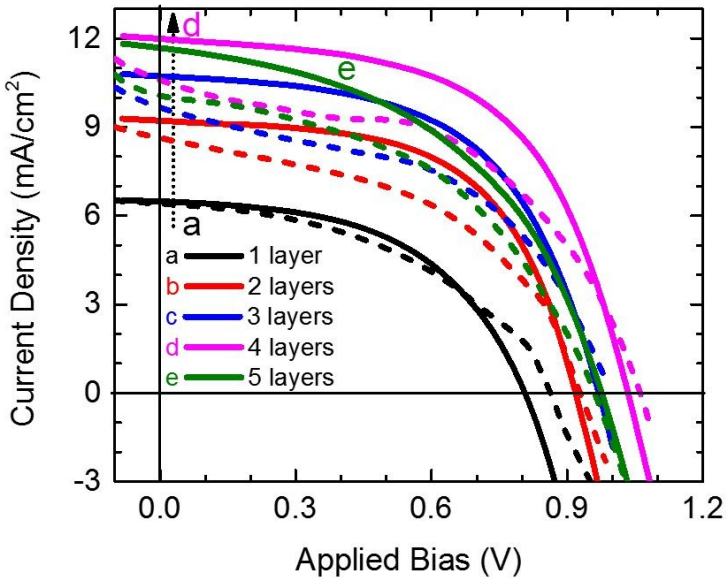

Figure S3. J-V curves measured under forward (dashed line) and reverse scans (straight line) of PQDSCs prepared from a QD solution of 50 mg/ml as function of the number of deposited layers.

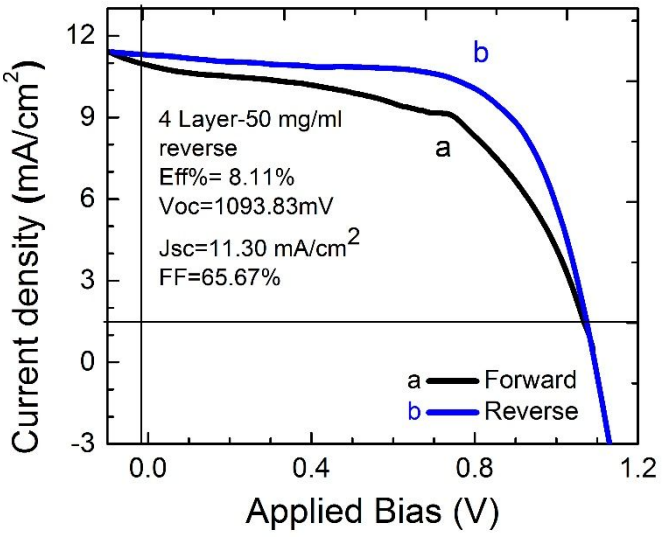

Figure S4. J-V curve measured under forward and reverse scans, of the champion cell fabricated in this study.

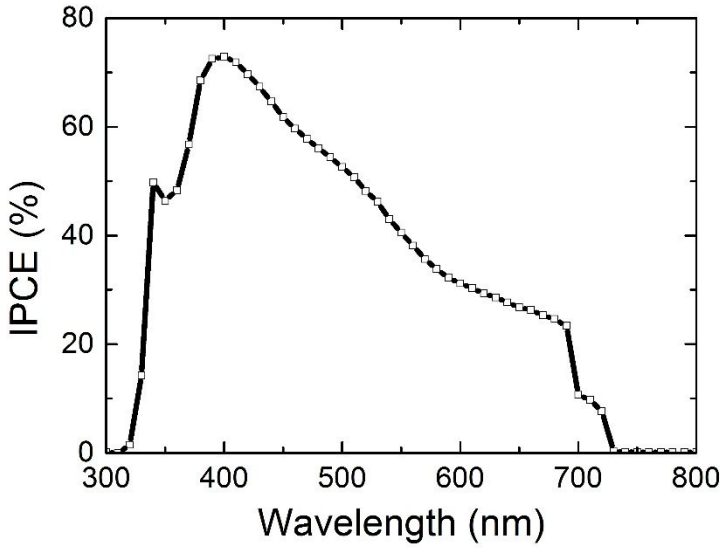

Figure S5. Example of the IPCE measured for the fabricated PQDSCs, from same champion cell fabricated in this study.

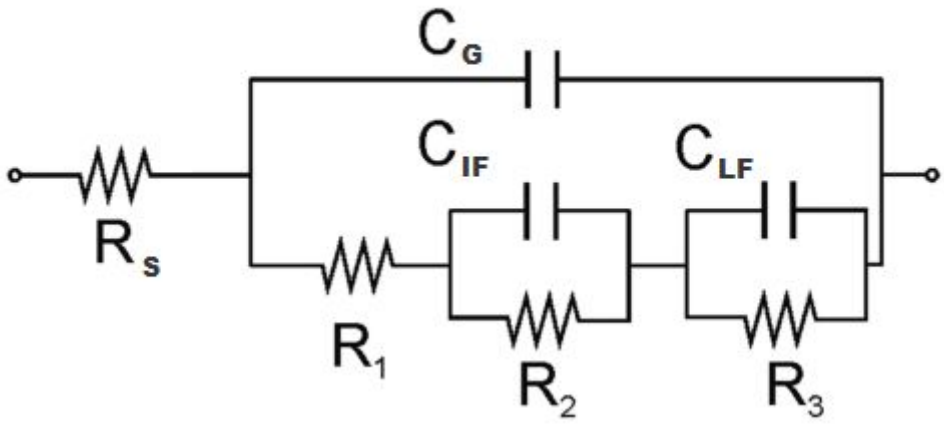

Figure S6. Equivalent circuit used for fitting the IS experimental data.[3] R_s is the series resistance originated by wires, connections and FTO sheet. C_G is the geometric capacitance of the device at high frequency. C_{IF} is the intermediate frequency capacitance. C_{LF} is the low frequency capacitance, associated with an accumulation capacitance of majority carries mediated by the presence on mobile ions.[4, 5] Interpretation of the physical meaning of R_1, R_2 and R_3 is not straight forward. The sum of all resistances provide the DC resistance, $R_{DC} = R_1+R_2+R_3+R_s$, where R_{DC} is the inverse of the slope of the current-voltage, J-V, curve. R_1 and R_2 are the responsible of the high frequency feature observed in Figure 3b, that contains information about transport resistance in the selective contacts.[3, 6] J-V curve reconstruction from impedance measurements suggest that recombination resistance, R_{rec}, cannot be directly related with low frequency resistance, R_3, but with the sum of high and low frequency resistances,[5, 7] analogously we have considered recombination resistance as $R_{rec} = R_{DC}-R_s$. Note that this expression overestimates R_{rec} as it includes a contribution from transport resistance at the selective contacts but still a valid approach for a qualitative comparison as selective contacts used in all the analyzed samples are the same.

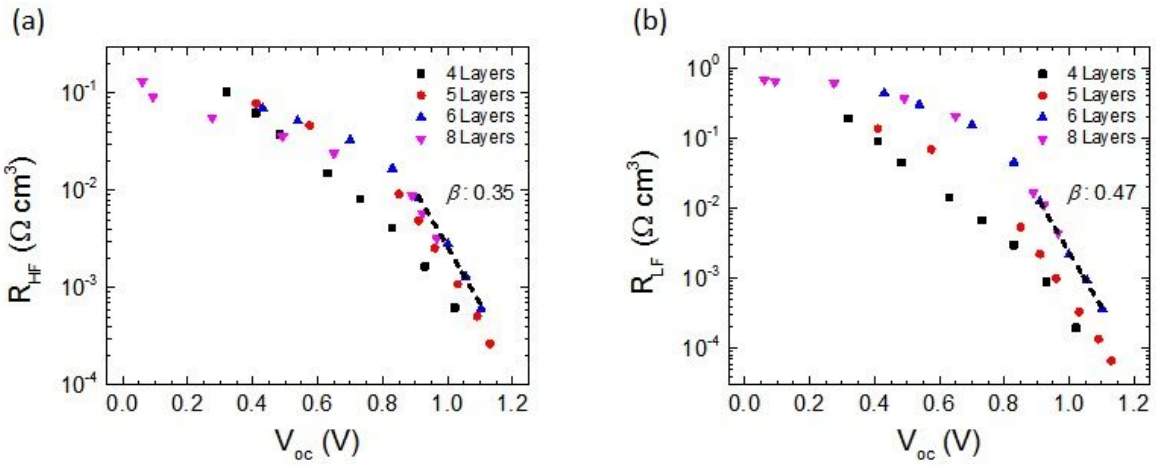

Figure S7. (a) High frequency resistance, $R_{HF} = R_1+R_2$ and **(b)** Low frequency resistance, $R_{LF} = R_3$ used in the determination of recombination resistance, $R_{rec} = R_1+R_2+R_3$ in Figure 3c. The β value obtained for thicker samples at high voltage is indicated. R_H, R_{LF} and R_{rec} present relatively

similar β values in good agreement with the β=1/m=0.42 value obtained from the dependence of the voltage with the light intensity, Figure 3a.

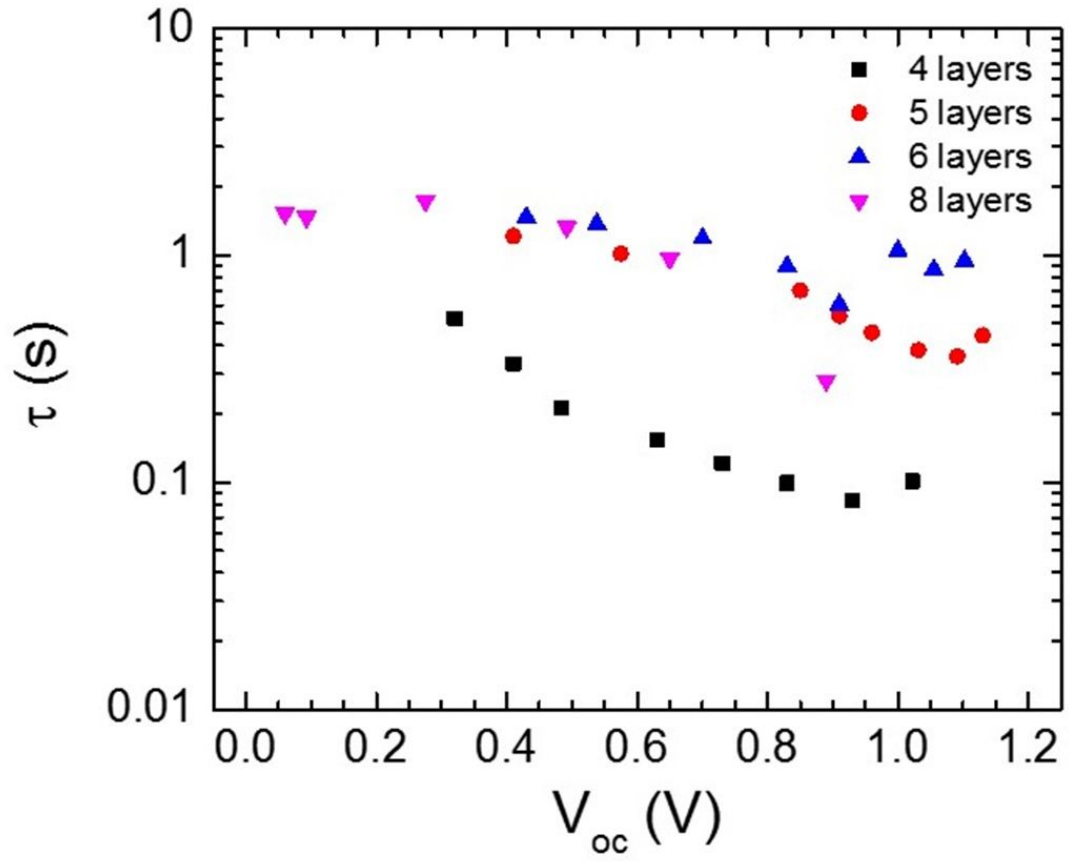

Figure S8. Characteristic time obtained as $\tau = C_{LF} \cdot R_{rec}$ from the data in Figure 3. In a good solar cell high R_{rec} are observed, consequently τ mainly depends on C_{LF}. C_{LF} has been related with the device hysteresis decreasing when hysteresis decrease,[8] as in inverted solar cells. In this context τ could be a good parameter to describe a perovskite solar cells as it is practically independent of the applied voltage and on the illumination.[9] However, a clear determination of the physical meaning of C_{LF} is needed in order to provide τ with a physical insight beyond a mere phenomenological parameter.

REFERENCES

(1) Sanehira, E. M.; Marshall, A. R.; Christians, J. A.; Harvey, S. P.; Ciesielski, P. N.; Wheeler, L. M.; Schulz, P.; Lin, L. Y.; Beard, M. C.; Luther, J. M. Enhanced mobility $CsPbI_3$ quantum dot arrays for record-efficiency,

high-voltage photovoltaic cells. *Sci. Adv.* **2017**, *3*, eaao4204.
(2) Pitarch-Tena, D.; Ngo, T. T.; Vallés-Pelarda, M.; Pauporté, T.; Mora-Seró, I. Impedance Spectroscopy Measurements in Perovskite Solar Cells: Device Stability and Noise Reduction. *ACS Energy Lett.* **2018**, *3*, 1044-1048.
(3) Guerrero, A.; Garcia-Belmonte, G.; Mora-Sero, I.; Bisquert, J.; Kang, Y. S.; Jacobsson, T. J.; Correa-Baena, J.-P.; Hagfeldt, A. Properties of Contact and Bulk Impedances in Hybrid Lead Halide Perovskite Solar Cells Including Inductive Loop Elements. *J. Phys. Chem. C* **2016**, *120*, 8023-8032.
(4) Zarazua, I.; Bisquert, J.; Garcia-Belmonte, G. Light-Induced Space-Charge Accumulation Zone as Photovoltaic Mechanism in Perovskite Solar Cells. *J. Phys. Chem. Lett.* **2016**, 7, 525-528.
(5) Zarazua, I.; Han, G.; Boix, P. P.; Mhaisalkar, S.; Fabregat-Santiago, F.; Mora-Seró, I.; Bisquert, J.; Garcia-Belmonte, G. Surface Recombination and Collection Efficiency in Perovskite Solar Cells from Impedance Analysis. *J. Phys. Chem. Lett.* **2016**, 7, 5105-5113.
(6) Juarez-Perez, E. J.; Wußler, M.; Fabregat-Santiago, F.; Lakus-Wollny, K.; Mankel, E.; Mayer, T.; Jaegermann, W.; Mora-Sero, I. Role of the Selective Contacts in the Performance of Lead Halide Perovskite Solar Cells. *J. Phys. Chem. Lett.* **2014**, *5*, 680-685.
(7) Zarazúa, I.; Sidhik, S.; Lopéz-Luke, T.; Esparza, D.; De la Rosa, E.; Reyes-Gomez, J.; Mora-Seró, I.; Garcia-Belmonte, G. Operating Mechanisms of Mesoscopic Perovskite Solar Cells through Impedance Spectroscopy and J–V Modeling. *J. Phys. Chem. Lett.* **2017**, *8*, 6073-6079.
(8) Kim, H.-S.; Jang, I.-H.; Ahn, N.; Choi, M.; Guerrero, A.; Bisquert, J.; Park, N.-G. Control of I–V Hysteresis in CH3NH3PbI3 Perovskite Solar Cell. *J. Phys. Chem. Lett.* **2015**, *6*, 4633-4639.
(9) Zarazua, I.; Han, G.; Boix, P. P.; Mhaisalkar, S.; Fabregat-Santiago, F.; Mora-Seró, I.; Bisquert, J.; Garcia-Belmonte, G. Surface Recombination and Collection Efficiency in Perovskite Solar Cells from Impedance Analysis. *J. Phys. Chem. Lett.* **2016**, 7, 5105-5113.